Carrier dynamics in InAs/GaAs submonolayer stacks coupled to Stranski-Krastanov quantum dots

Thomas Switaiski* and Ulrike Woggon†
Institut für Optik und Atomare Physik, Technische Universität Berlin, Straße des 17. Juni 135, 10623 Berlin, Germany.

Dorian E. Alden Angeles, Axel Hoffmann, Jan-Hindrik Schulze, Tim David Germann, André Strittmatter, and Udo W. Pohl
Institut für Festkörperphysik, Technische Universität Berlin, Hardenbergstraße 36, 10623 Berlin, Germany.
(Received 25 March 2013; revised manuscript received 2 July 2013; published 25 July 2013)

Time-resolved photoluminescence experiments on a coupled system of Stranski-Krastanov quantum dots (SK QDs) overgrown by a stack of submonolayer (SML) depositions reveal an acceleration of the carrier dynamics in the SML stack mediated by distance-dependent transfer processes. The coupling between an SML stack and an SK QD layer increases with decreasing spacer thickness d, which separates the two different nanostructure systems. This control parameter d as well as the optical transition energies of the SML stack can be adjusted via the growth process. The observed photoluminescence dynamics of the combined SK QD and SML system is well described by a rate equation model which includes both pure zero-dimensional and zero-dimensional–two-dimensional states.

DOI: 10.1103/PhysRevB.88.035314 PACS number(s): 78.47.jd, 78.55.Cr, 78.67.Hc, 78.67.Pt

I. INTRODUCTION

Quantum confinement in semiconductor nanostructures is an established approach to fabricate novel materials. Quantum dots (QDs), for example, allow for tuning the emission wavelength from UV to near infrared (NIR);[1–6] they exhibit long coherence lifetimes[7] and are widely used in lasers and amplifiers providing low-threshold currents, high-temperature stability, and ultrafast gain dynamics.[8–11] Recent developments include periodic stacking of submonolayer (SML) superlattices[12–15] and strain-induced SML depositions on Stranski-Krastanov (SK) QDs to form columnar quantum dots.[16–19] A natural next step is the design of combinations of nanostructures of different dimensionalities, such as coupled zero-dimensional–two-dimensional (0D-2D) structures.[20] Advanced 0D-2D designs offer tuning of energy and radiative lifetimes as well as density of states and scattering times.

In this work we present an InAs/GaAs quantum system which consists of an SK QD layer coupled to a stack of InAs SMLs embedded in GaAs. The SK QD layer and the SML stack are separated by a GaAs spacer layer of varying thickness d. Such a coupled system of SK QDs and an SML stack comprises 0D and 2D energy states with tunable confinement, density of states, and energy overlap, as illustrated in Fig. 1.

A submonolayer is a deposition of material with an amount less than needed to form one crystal layer. Stacked InAs SML depositions with thin separating GaAs matrix layers (few monolayers) offer tunable energies, as their recombination energy can be controlled by the period, number of cycles, and ratio of InAs and GaAs thickness of the superlattice structure.[15,21] The energy of the whole SML stack is essentially determined by the GaAs barrier thickness between each single SML. The size, and thus the energies, of the SK QDs can be controlled by growth parameters. In particular, the ground state of the SML stack can be tuned in resonance to the excited states of the SK QDs. The energy overlap and the spatial proximity enable the interaction between the SK QD system and the SML stack. A motivation for the study of SK QDs which act as a seed for SML structures on top is an expected self-ordering during SML growth by the strain field induced by the SK QDs.[22,23] Furthermore, the small inhomogeneous broadening of an SML stack allows a precise tuning of the optical transition energies and, e.g., of the spectral gain to resonator modes. Hereby the entire volume of the active medium can contribute to the gain, allowing for high-power lasers and high-speed surface-emitting lasers, as demonstrated with InAs/GaAs SML stacks.[24–30]

In the following, we will show that the SML recombination dynamics is remarkably governed by state filling and Pauli blocking of states arising from both 0D and 2D densities of states. The photoluminescence (PL) dynamics becomes fully controlled by populating and saturating the 0D resonances via energy relaxation from the SML stacks to the SK QD ground state. As a consequence, the SML dynamics is accelerated compared to a reference SML stack without underlying SK QDs. The temporal onset and the degree of the PL decay fastening can be controlled by the spacer thickness d and the excitation power P_{ex}. Hence, the here presented nanostructure concept allows for both tuning of energies and populations, as sketched in Fig. 1.

II. SAMPLES AND EXPERIMENTS

The 0D-2D samples presented here are InAs/GaAs SML stacks with a single underlying InGaAs SK QD layer, grown using metalorganic vapor-phase epitaxy (MOVPE). The structural properties of similar samples were studied by Lenz *et al.*[21] and Niermann *et al.*[14] using high-resolution microscopy techniques. The cross-section scanning tunneling microscopy (XSTM) images made by Lenz *et al.* show indium-rich agglomerations, which are laterally embedded in an alloy of low indium content. They reported evidence that the SML stack PL originates from both 0D and 2D localized states, resulting in a high-energy tail in the PL spectrum.[21]

The studied samples were grown on (001)-oriented GaAs substrates. $In_{0.84}Ga_{0.16}As$ quantum dots were grown at $T = 500\,^{\circ}C$ in the Stranski-Krastanov mode and covered with a spacer layer of thickness d (varied from 0.75 to 5 nm).

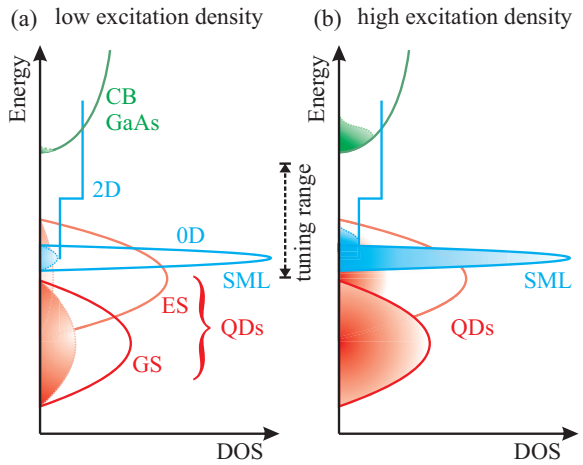

FIG. 1. (Color online) Scheme of the overlap of the QDs and SML stack densities of states (DOS). Excited and ground states of the QDs are denoted by ES and GS. An SML stack includes 2D and 0D states. Populations are indicated by shaded areas for (a) low and (b) high excitation density. The tuning range of the transition energy in the SML stack is indicated by the dashed vertical arrow.

Then a stack of InAs SML comprising 10 cycles of 0.5 monolayer (ML) InAs and 2 ML GaAs was deposited on top. The entire structure was sandwiched by AlGaAs barriers to prevent escape of photoexcited carriers. The actual value of the separation between the QDs and the SML stack is assumed to be somewhat smaller than the nominal value d [reduced by the height of the QDs; see sample structure in the inset in Fig. 2(a)]. Reference samples were grown which contain either an SML stack or a single layer of SK QDs.

Room-temperature PL was measured using a frequency-doubled Nd:YAG laser in cw mode with a wavelength of 532 nm as the excitation source. The detection system comprised a spectrometer and a germanium detector.

Photoluminescence excitation (PLE) measurements were performed utilizing a cw mode and tunable Ti:sapphire laser as the excitation light source. The laser was modulated with a chopper at a frequency of 69 Hz and then focused on the sample placed inside a liquid-helium flow cryostat in a 45° angle to the excitation axis. The emitted light was guided through a double-monochromator system and detected by a germanium pin diode. Additionally, to suppress undesired noise sources, the output voltage was connected to a lock-in amplifier which was synchronized with the modulation frequency of the chopper. For PLE measurements, the detection energy, set by a double monochromator, was fixed to a specific energy, and the excitation energy of the Ti:sapphire laser was varied between 1.49 and 1.24 eV. PLE is used to measure the density of absorbing states and the efficiency of relaxation channels by detecting luminescence at a predetermined specific energy, e.g., the energetically lowest resonance, thereby gaining information about energy-transfer processes.

For time-resolved PL measurements the samples were excited by a Ti:sapphire laser operating at 770 nm with a 150-fs pulse length and 75.4-MHz repetition rate. The emitted light was dispersed in a spectrometer and detected by a Hamamatsu streak camera, which is optimized for detection

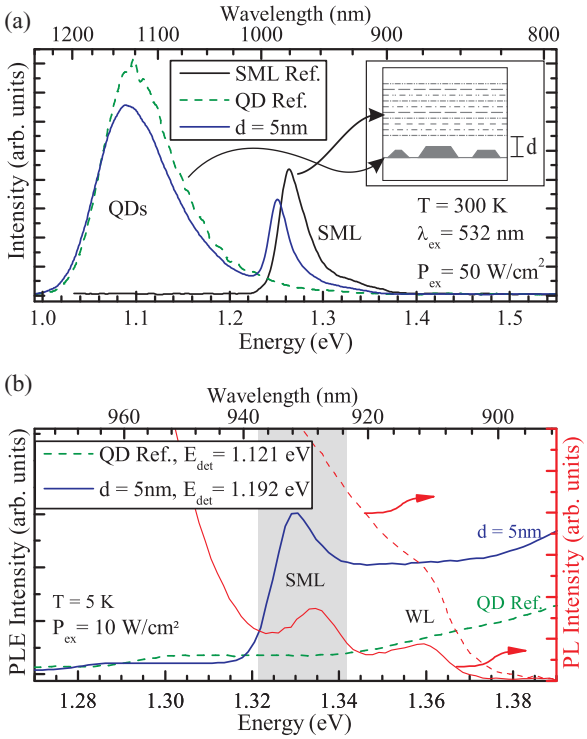

FIG. 2. (Color online) (a) Exemplary spectra of room-temperature photoluminescence from samples containing only SML (black solid line), only QDs (green dashed line), and SML and QDs separated by a spacer layer of $d = 5$ nm (blue solid line). Inset: scheme of the sample structure. (b) PLE and PL spectra from the QD reference sample (PLE: green dashed line, PL: red dashed line) and sample with $d = 5$ nm (PLE: blue solid line, PL: red solid line) at low temperature showing an additional excitation channel into the QDs, which is introduced by the SML stack insertion. Detection energy is set to the respective maximum of the SK QD PL. At low temperatures, luminescence from the wetting layer (WL) of the SK QDs is observed.

in the near infrared. The full width at half maximum of the instrument response function is 25 ps. For measurements at low temperature the samples were mounted in a liquid-helium flow cryostat.

III. RESULTS AND DISCUSSION

A. Excitation density dependence of photoluminescence

Figure 2(a) shows exemplary emission spectra of the combined 0D-2D nanostructure and the respective reference samples. The parameter which controls the interaction is the spatial separation of the SML stack from the SK QD layer which is realized by a spacer layer of thickness d [see scheme in the inset of Fig. 2(a)]. Luminescence of the GaAs matrix (maximum at 1.41 eV, not visible at the low excitation intensity applied), the SML stacks (1.26–1.21 eV, depending on spacer thickness d), and the SK QDs (1.06–1.1 eV) is observed. The PL of the SML stack reveals a small linewidth of about 20 meV at room temperature and below 10 meV at low temperature. An asymmetric line shape with a high-energy tail is observed in the spectrum of the SML stacks.

Figure 2(b) displays PLE spectra of the sample containing only SK QDs (QD reference sample) and the sample with an SML stack separated by a spacer layer of $d = 5$ nm from a single layer of SK QDs. The detection energy is set to the respective maximum of the SK QD PL (1.121 eV for the QD reference sample and 1.192 eV for the sample with $d = 5$ nm). In these spectra the impact of the SML stack insertions on the excitation properties of the SK QDs is clearly visible. An absorption maximum at 1.330 eV (resonant to the SML energy) is observed for the $d = 5$ nm sample. In contrast, the QD reference sample does not exhibit this feature. Comparing the samples and their corresponding PL as well as PLE spectra, it is clear that the absorption occurs due to the presence of the SML structure. This shows that a carrier transfer from the SML stack into the SK QDs takes place, where then radiative recombination occurs. According to this, an additional excitation and relaxation channel into the SK QDs is introduced by the insertion of the SML stack.

Next we discuss cw power series of SK QD-seeded SML stacks and investigate the photoluminescence spectrum for four spacer values of $d = 0.75$, 1.5, 3, and 5 nm. In Fig. 3(a) the PL spectra excited at the low excitation intensity of 5 W cm^{-2} are presented for all samples, including the QD and SML reference samples. The luminescence from the SML stack clearly depends on the spacer thickness d. In the absence of an SK QD layer its recombination energy is highest. With decreasing spacer d, the recombination energy and the PL intensity of the SML stack decrease. The QD luminescence shows a systematic redshift as well as a drop in intensity, which both correlate to the spacer thickness d.

The dependence on excitation intensity, spanning four orders of magnitude, is presented in Figs. 3(a) to 3(d). In the PL spectra with low excitation density there is no luminescence visible from the GaAs matrix. This indicates that relaxation channels into the SML stack and QDs dominate over recombination pathways within the GaAs barrier itself.

At high excitation power density, a feature on the high-energy side of the SML PL can be observed as marked by a star in Figs. 3(b) to 3(d). A similar feature appears in the spectrum of the QD reference sample and is likely due to a defect introduced during sample growth.

The excitation-dependent integral PL intensities are shown in Fig. 4. The slopes k in the double-logarithmic plot are equal to the exponent k in such a type of $I_{\mathrm{PL}} \propto (P_{\mathrm{ex}})^k$ presentation and contain the information about the density of available QD and SML states which may contribute to the overall recombination of the combined SK QD/SML stack. A linear dependence on the excitation density P_{ex} will result in a slope $k = 1$ in the double-logarithmic plot and gradual population saturation in a slope $k < 1$. In the double-logarithmic plot, the PL from the SML stacks is increasing with the excitation density, while the quantum-dot PL shows a saturation for all samples above 500 W cm^{-2}. This indicates a larger density of radiative states in the SML stack than in the QD ensemble. Furthermore, the slope is steeper for the SMLs, and no saturation is observed for the applied continuous-wave excitation densities. Fitting the excitation density dependence of the PL intensities yields slopes k for the QDs smaller than 1 (at low excitation intensities, for the range from 5 to 500 W cm^{-2}) and for the SML stacks k is around 1.3 (for all

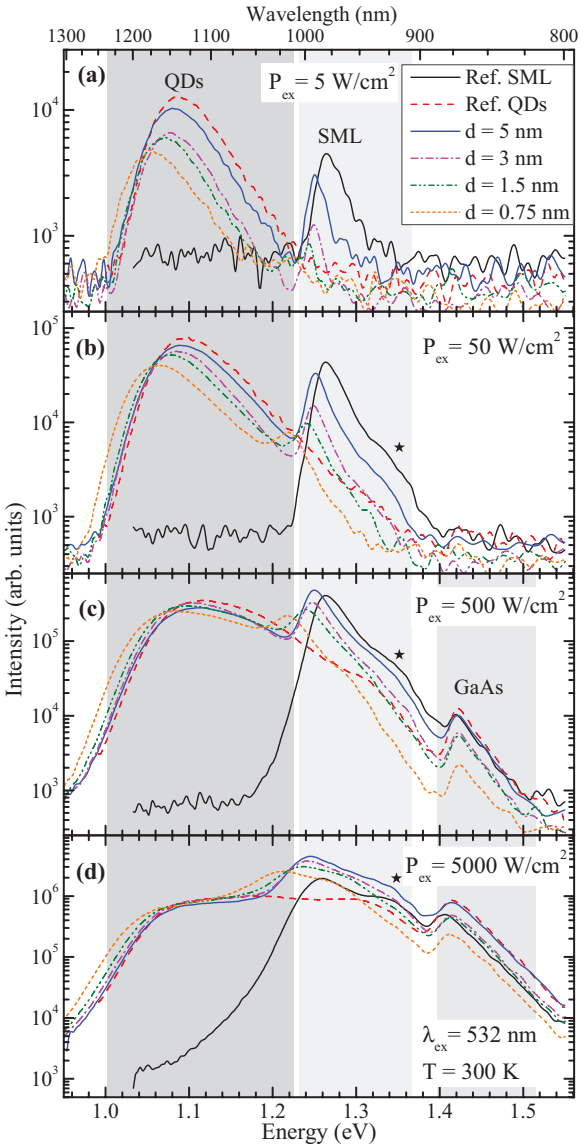

FIG. 3. (Color online) Room-temperature photoluminescence (cw excited) from the studied samples shown for increasing excitation power P_{ex} from top to bottom. The peaks are assigned to QD, SML, and GaAs emission (marked by shaded areas). The feature marked with a star is assigned to defect-related emission, as it occurs in both types of samples.

excitation intensities). For the SML reference sample a slope $k = 1.0$ is derived, showing a strict linear power dependence, which is not saturable in this density range. The QD reference sample gives $k = 0.8$, representing a less than linear power dependence. The increase of k by coupling an SML stack to a layer of SK QDs from 1.0 to 1.3 can be explained with the introduced energy-transfer channel into the SK QDs. At low excitation densities the relaxation from the SML stack into SK QDs is dominant, resulting in a reduced PL intensity. But increasing the excitation intensity leads to filling of a non-negligible amount of SK QD states. And Pauli blocking reduces the transfer rate of carriers from the SML stack into SK QDs. That leads to an effective, nonlinear increase of the PL intensity from the SML stack. The smaller value derived here

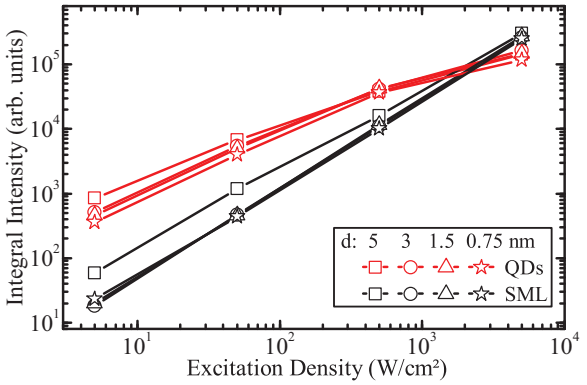

FIG. 4. (Color online) Excitation power dependence of the SK QDs (red) and SML (black) integrated PL emission for different spacer thicknesses d.

for the density of states (DOS) of the QD states affects the SML recombination dynamics: it should be remarkably governed by state filling and Pauli blocking of QD states. Therefore we expect a photoluminescence dynamics which is controlled by populating and saturating the QD resonances via energy relaxation from the SML stacks to the SK QD ground state.

B. Dependence of the radiative recombination on SML-QD coupling

The PL dynamics of the described SML nanostructures after pulsed excitation with 150-fs pulses at 770 nm ($E = 1.6$ eV, i.e., off resonant above the GaAs band gap) was investigated using the spatial separation of an SML stack from an SK QDs layer as the external control parameter, which is realized by spacer thickness d. Figure 5 shows transients of the SML PL, which were derived from streak camera images measured at $T = 15$ K. Additionally, the PL dynamics of the SML reference sample, which only contains an SML stack, is plotted in Fig. 5. For low excitation density, the SML dynamics of all samples can be described by monoexponential decays. While in the case of high excitation intensity the decay behavior of the SML reference sample is well described by a monoexponential decay, the observed dynamics of the samples containing SML stacks coupled to SK QDs cannot be assigned to a single monoexponential decay or superpositions of several monoexponential decays.

With decreasing spacer thickness d between the SK QD layer and the SML stack, the luminescence from the SML stack decays faster. The presence of a QD layer leads to an acceleration of the SML PL decay caused by the capture of carriers from the SML into the QDs. The rate of the transfer process from SML to QDs depends on the separation d of the two types of nanostructures. The higher the transfer rate is, the more carriers are transferred into the QDs. Obviously, the coupling between the SML stack and the SK QDs, which is controlled by the spacer thickness d, has a strong effect on the dynamics in the SML stack.

The visible convex shape of the PL dynamics can be explained by the Pauli exclusion principle, as the SK QDs have only a limited number of states which can be occupied via carrier relaxation from the SML stack or the GaAs matrix. The Pauli blocking of relaxation into already occupied states

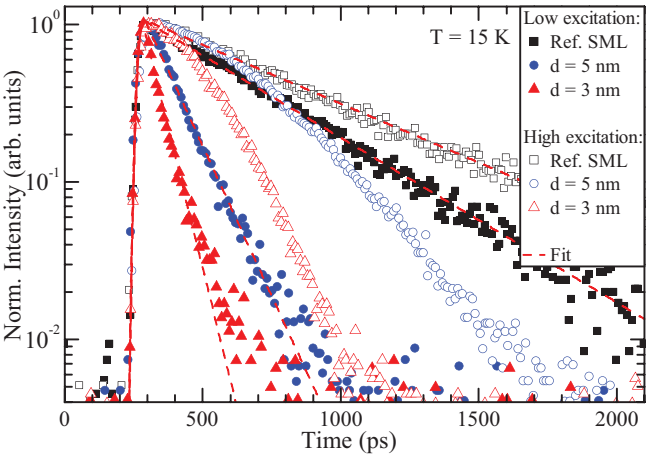

FIG. 5. (Color online) Time-resolved PL measured at the spectral position of the PL maximum of the SML stack integrated over a 3-nm-wide spectral window at low temperature. The detection energy for low (high) excitation power of the reference SML stack is $E =$ 1.344 eV (1.345 eV), for $d = 5$ nm is 1.334 eV (1.336 eV), and for $d = 3$ nm is 1.333 eV (1.335 eV). Two excitation powers which differ by a factor of 10 are shown. Low (high) excitation is shown as solid (open) symbols. Monoexponential fits convoluted with the instrument response are plotted as dashed red lines. The resulting decay times from the fits are for low excitation: reference SML stack, 415 ps; $d = 5$ nm, 114 ps; $d = 3$ nm, 61 ps. For high excitation, the decay time for the reference SML stack is 580 ps (for others, see the text).

results in a time-dependent decay constant $\tau(t)$; i.e., the decay constant τ decreases with respect to the delay time t to the exciting laser pulse. Shortly after excitation (short delay, small t) with high excitation power, $\tau(t)$ is large, as shown in Fig. 5, because the carrier occupation of SK QDs is at maximum and Pauli blocking prevents carrier relaxation from the SML stack. Therefore the relaxation rate from the SML stack to the QDs is small, leading to a large effective time constant for this relaxation channel. Thus, for small delay times after excitation, radiative recombination is the dominant decay channel.

With increasing delay after excitation (long delay, large t) $\tau(t)$ decreases because now the QD population itself decreases with its radiative recombination rate of 800 ps. This leads to an increase of relaxation and an acceleration of the SML recombination dynamics. Here, the transfer into the QDs is the dominant decay channel. Therefore monoexponential fitting does not yield an adequate description of the dynamics, and a more complex rate equation system has to be developed for the observed dynamics to describe the interacting 0D-2D system of SK QDs and SML stacks.

C. Modeling the population dynamics

In this section we present a model which describes the dynamics of a combined SK QD and SML system that allows for engineering transfer and decay time constants. More simple descriptions with monoexponential, multiexponential, or stretched-exponential decays do not take into account the Pauli blocking. The scheme for the applied rate equation system (RES) is shown in Fig. 6. The time-dependent coupled populations of the energy levels depicted in

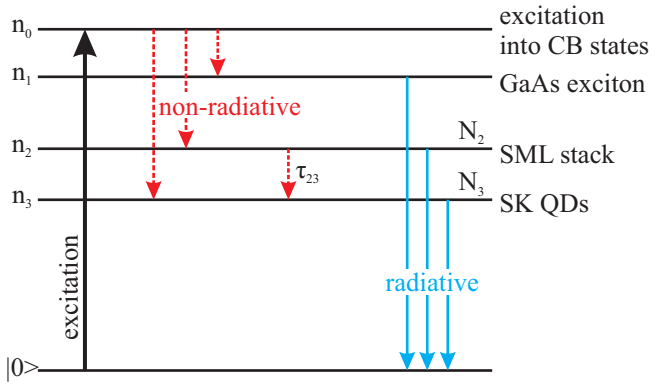

FIG. 6. (Color online) Scheme of the rate equation system showing the energy levels and the relaxation and recombination channels. n_i denotes populations of states. Red dashed arrows: nonradiative relaxation, blue arrow: radiative recombination, black arrow: excitation into the conduction band (CB).

Fig. 6 read

$$\dot{n_0}(t) = -\frac{n_0(t)}{\tau_{01}} - [1 - n_2(t)]\frac{n_0(t)}{\tau_{02}} - [N_3 - n_3(t)]\frac{n_0(t)}{\tau_{03}}, \tag{1}$$

$$\dot{n_1}(t) = \frac{n_0(t)}{\tau_{01}} - \frac{n_1(t)}{\tau_1}, \tag{2}$$

$$\dot{n_2}(t) = [1 - n_2(t)]\frac{n_0(t)}{\tau_{02}} - [N_3 - n_3(t)]\frac{n_2(t)}{\tau_{23}} - \frac{n_2(t)}{\tau_2},$$

$$\dot{n_3}(t) = [N_3 - n_3(t)]\frac{n_0(t)}{\tau_{03}} + [N_3 - n_3(t)]\frac{n_2(t)}{\tau_{23}} - \frac{n_3(t)}{\tau_3}. \tag{3}$$

Here, $n_i(t)$ is the population of state i, normalized with respect to the total number of states of the SML stack N_2. The indices i correspond to the excited free carriers in the GaAs ($i = 0$), to the excitons in GaAs ($i = 1$), to those in the SML stack ($i = 2$), and to those in the SK QDs ($i = 3$). N_3 is the number of occupiable states of the SK QDs, $\frac{n_3}{N_3}$ is the population probability for the SK QDs, τ_i is the radiative recombination time constant of state i, and τ_{ij} is the relaxation time constant from state i to j. Since the whole RES is normalized with respect to N_2, the Pauli-blocking term for n_2 is equal to unity, and N_3 is expressed in units of N_2. Thus, N_3 is the ratio of the total number of states of the SK QDs in comparison to those of the SML stack. $(1 - n_2)$ represents the finite number of available states for the SML stack, and $(N_3 - n_3)$ represents those for the SK QDs in the rate equation model. The relaxation from occupied states of the SML stack into unoccupied SK QD states is described by the time constant τ_{23}. The carrier transfer rate from the SML stack to the QDs depends on the population of the quantum dots (in particular $[N_3 - n_3(t)]$), the population $n_2(t)$ in the SML stack, and the time constant τ_{23}. The excitation by a laser pulse is given by the boundary condition $n_0(t = 0) = n_{00}$, where n_{00} is the initial population, in units of the total number of states of the SML stack N_2. The RES describes the QDs as an ensemble, instead of a single QD level. To simplify the RES, we do not distinguish between ground and excited states for the QD ensemble or the SML stack.

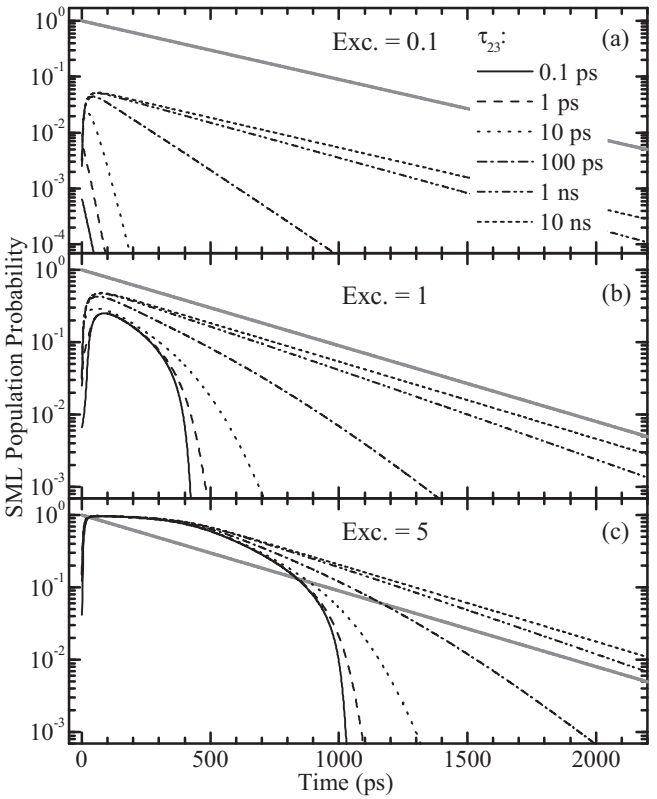

FIG. 7. Numerical solution of the modeled RES for the combined SK QD/SML stack samples with varying time constant τ_{23} indicating the d-dependent transfer efficiency. Three different excitation densities are plotted in units of the number of states of the SML stack; see the text. The gray straight line is a guide for the eye; it represents monoexponential decay with a time constant equal to the observed PL decay of the SML reference sample.

The parameters of the RES were chosen according to our measurements: observed rise times into the SML stack and SK QDs $\tau_{02} = \tau_{03} = 30$ ps, the observed rise time of the GaAs PL $\tau_{01} = 200$ ps (capture from GaAs conduction band), and observed radiative time constants $\tau_1 = 1.3$ ns, $\tau_2 = 0.415$ ns, as measured for the reference SML sample at the low temperature of 15 K, and $\tau_3 = 0.8$ ns. In the RES we do not take into account inhomogeneous broadening and assume a uniform radiative lifetime of 800 ps for the SK QDs. This value is consistent with our experimental findings from time-resolved PL measurements of the QD ground state in the reference sample. We assume a larger density of states for the SMLs compared to the SK QDs, i.e., $N_{QD} < N_{SML}$ and thus $N_3 < 1$. According to the results of the power dependencies shown in Fig. 4, at the highest excitation density the PL intensity from the SML stacks is about twice that of the SK QDs. Additionally, the slopes k of the PL differ by a factor of about 0.6 in the case of 5- and 3-nm-thick spacers d. Therefore we chose $N_3 = 1/2$ in the following simulations.

Figure 7 shows numerical solutions of the RES for three different excitation densities with varying τ_{23} covering five orders of magnitude. The excitation is given in units of the number of states in the SML stack N_2. For example, an excitation of 1 is the generation of a number of free carriers equal to the number of states inside the SML stack. The

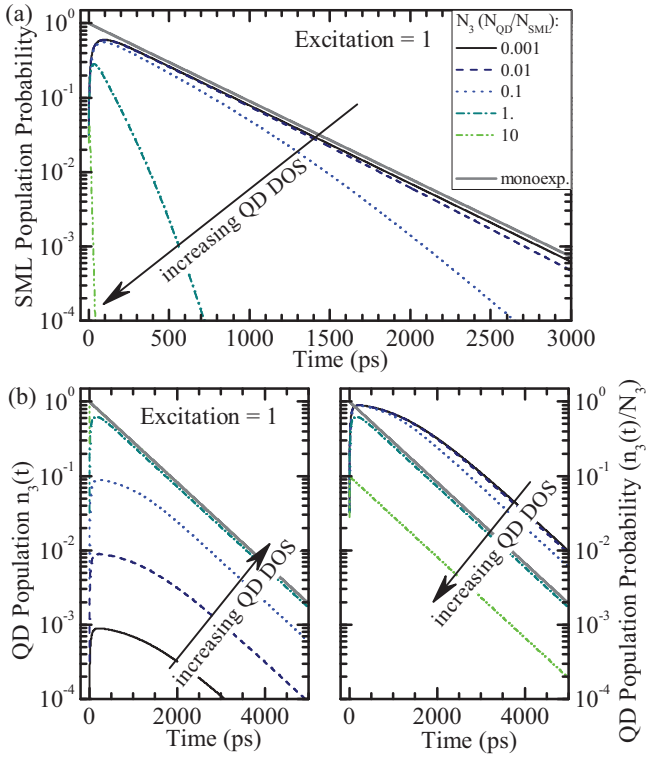

FIG. 8. (Color online) Numerical solutions of the RES for (a) the SML stack $n_2(t)$ and (b) the SK QDs $n_3(t)$ for a wide range of number of states N_3 of the SK QDs. N_3 varied from 0.001 to 10. Because QD population $n_3(t)$ (left) and QD population probability $n_3(t)/N_3$ (right) are linked by the factor N_3^{-1}, they show opposite trends when varying the SK QD DOS. $n_3(t)$ is proportional to the emitted PL, while $n_3(t)/N_3$ is the ratio of occupied QD states to the whole SK QD DOS. The gray straight lines are guides for the eye; they represent monoexponential decays with time constants equal to the observed PL decay of the SML and QD reference samples.

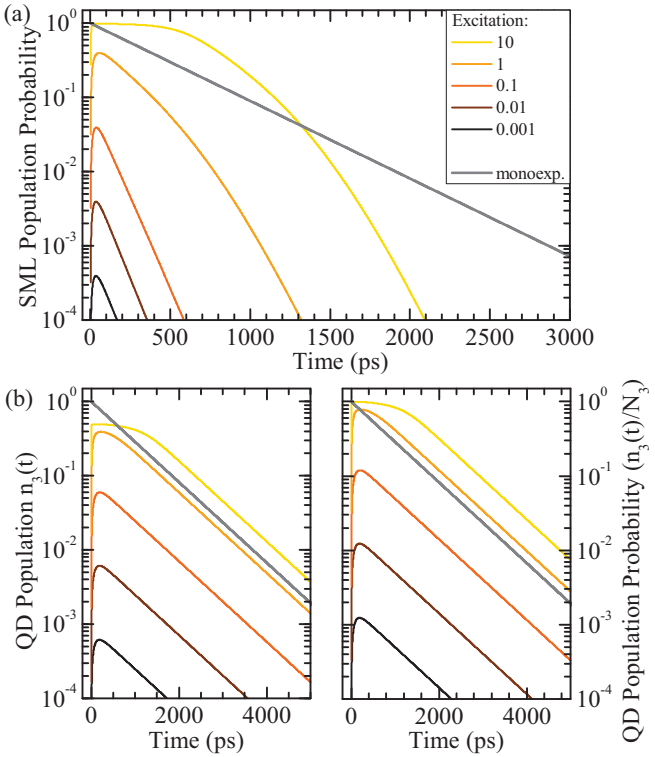

FIG. 9. (Color online) Numerical solutions of the RES for (a) the SML stack $n_2(t)$ and (b) the SK QDs $n_3(t)$ for a wide range of different excitation densities $n_0(t=0)=n_{00}$, varied from 0.001 to 10. The QD population and QD population probability show the same trends, as the factor N_3^{-1} is constant here. The gray straight lines are guides for the eye; they represent monoexponential decays with time constants equal to the observed PL decay of the SML and QD reference samples.

dynamics are strongly influenced by the excitation density $n_0(t=0)$ and the transfer time constant τ_{23}. In particular for the case where the excitation equals 1, the decay time and the maximum population strongly depend on the transfer time constant, resulting in a decrease of PL emission intensity with decreasing τ_{23}. For the higher excitation densities, the initial dynamics are mainly influenced by the excitation density and Pauli blocking of the energetically lower QD levels. This leads to a saturation plateau right after excitation. After depletion of the plateau, the decay depends on the transfer time constant τ_{23}. For large τ_{23} the dynamics converge to a monoexponential decay with a time constant equal to the observed radiative lifetime of the uncoupled case. As we can see in Fig. 7 for higher excitation densities (excitation of 5), after a long-lasting population saturation plateau a monoexponential decay is possible for large τ_{23} times.

The influence of the QD total number of states N_3 on the recombination dynamics, over four orders of magnitude, is shown in Fig. 8. With increasing N_3, a faster decay of the SML population occurs. This leads to a decrease of the integral under the transient, i.e., the time-integrated PL intensity. Furthermore, an increase of the total QD population n_3 but a decrease of the QD population probability n_3/N_3 is observed. Increasing the total number of radiative states N_3 of the QDs results in an increased transfer rate since the Pauli-blocking term $[N_3 - n_3(t)]$ is reduced. Therefore the transfer process from the SML stack to the QDs becomes more efficient. For small N_3 a saturation plateau can be observed in the QD dynamics.

Increasing the excitation density $n_0(t=0)$ reveals the saturability of the whole system, as illustrated in Fig. 9. For very low excitation densities (<0.1) saturation effects do not occur in the transients of either the SML stack or the SK QDs. As the population probabilities reach only small values (10^{-1} and below), the Pauli-blocking terms ($[1 - n_i(t)] \approx 1$) are negligible. As shown in the scheme in Fig. 1(a), the carriers accumulate in the SK QD ground state, which is the energetically lowest state, and the QD PL dominates the spectrum.

When the QD population probability reaches larger values ($>10^{-1}$), the rate of the relaxation channel from the SML stack to the QDs is governed by the Pauli-blocking term ($[1 - n_3(t)] < 1$). This bottleneck leads to a convex bowing in the SML stack dynamics, as the relaxation rate into the SMLs decreases and the radiative recombination gains significance for the decay. After depletion of the QD saturation, the relaxation rate from the SML increases and dominates the SML dynamics.

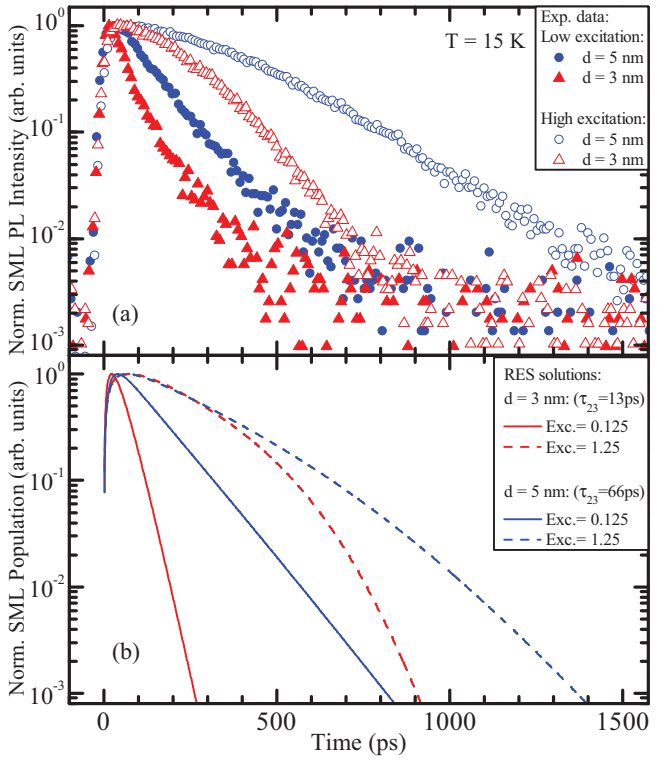

FIG. 10. (Color online) (a) Measured SML PL transients of combined SML stack/SK QD samples. (b) Numerical solution of the modeled RES for the combined SML stack/SK QD samples with different time constants τ_{23} and excitation powers to simulate the experimental decay curves. The factor between excitation powers is 10 (also for the experimental data). Blue: $\tau_{23} = 66$ ps for a sample with $d = 5$ nm; red: $\tau_{23} = 13$ ps for $d = 3$ nm.

High excitation densities (>1) result in saturation of the QD states, which is visible as a plateau in the population probability [see Fig. 1(b)]. As there are no free states in the QD ensemble, blocking of the relaxation channel from the SML stack occurs, mediated by $[1 - n_3(t)] = 0$. After depletion, the dynamics are dominated by the transfer channel into the QDs.

D. Experimental results for the spacer d and power P_{ex} dependent dynamics

For comparison of our simulation results of Figs. 7 to 9 with the experimental data, transients from the streak measurements are included in Fig. 10, which shows numerical solutions of the RES for the SML stack with different time constants τ_{23} to simulate the transient data. The transfer time constant τ_{23} is approximated to be in the range of 66 ps for the case of $d = 5$ nm and 13 ps for $d \leqslant 3$ nm. A small value for τ_{23} is connected to a larger transfer rate.

The additional relaxation channel, introduced by the QD layer, is faster than the radiative recombination of the SML stack itself and can therefore not be neglected. Numerical solutions of the rate equation system showed that even large transfer time constants $\tau_{23} \sim 1$ ns will lead to observable changes in the dynamics; see the theoretical results of Fig. 7.

The experimental results give evidence that the coupling between SK QDs and the SML stack is tunable by changing the spacer thickness d. This offers a parameter to control the decay time at the SML stack luminescence energy. In addition, as shown in previous work,[21] the recombination energy of the SML stack can be controlled by the period length of the SML stack superlattice. This enables us to tune the energy overlap of the densities of states, as indicated in Fig. 1. Thus, SML stacks with an SK QD layer are coupled systems with a combined 0D-2D density of states whose properties can be controlled by d and P_{ex} and allow engineering of the population of states and relaxation dynamics. The photoluminescence dynamics becomes fully controlled by populating and saturating the 0D resonances via energy relaxation from the SML stacks to the SK QD ground state.

E. Energy-transfer efficiency

The system we are investigating resembles donor-acceptor systems in molecular energy-transfer processes. If the emission of the donor molecule is resonant to the absorption of the acceptor molecule, the donor transfers energy via a dipole-dipole interaction to the acceptor. Such fluorescence resonance energy transfer (FRET) is widely used to measure the distance between two molecules.[31] It is tempting to test the capacity of the FRET concept to estimate the spatial transfer distance between SML stacks and the SK QD layer. By applying the FRET concept to semiconductor nanostructures, the distance between two nanostructures (NS) could be measured by determining the energy-transfer efficiency. This can be done by measuring the emission intensities (or the luminescence lifetimes) of the energy-donating NS for the unperturbed case as a reference and for the coupled case.

We can characterize our samples with the transfer efficiency[32] $E_{\text{transfer}} = 1 - \tau_{DA}/\tau_D$. τ_D is the reference SML stack PL lifetime, and τ_{DA} is the decay time of the SML stack in the presence of SK QDs. Here, we have to use values for low excitation densities because for high excitation densities the described saturation effects occur. Inserting the decay times for low excitation (see Fig. 5), we derive transfer efficiencies E_{transfer} of 73% for separation $d = 5$ nm and 85% for $d = 3$ nm. Thus the characteristic spacer thickness, for which the efficiency equals one half, is larger than 5 nm. It is not clear if the transfer dependence on the separation d is exponential like in the case of charge-carrier tunneling or a polynomial to the sixth power as in the case of FRET interaction. Therefore, for clarification of the nature of the transfer process, experiments on the dynamics of SML stacks coupled to SK QDs with a wider range of different separations d, in particular larger than 5 nm, are required.

IV. SUMMARY

We presented a combined system of two different nanostructures made by coupling an SML stack to a layer of SK QDs. The energy structure and the coupling strength can be engineered, allowing for tuning the decay dynamics. Evidence for the transfer of charge carriers was found in PLE, PL, and time-resolved PL measurements, and we were able to describe the observed dynamics with a RES considering this transfer. Coupling an SML stack to a layer of SK QDs introduces an additional decay channel for the localized charge carriers.

This accelerates the population decay inside an SML stack. The strong interaction of an SML stack with an SK QD layer should lead to a fast refill of empty QD states, resulting in a fast gain recovery for the QDs. Coupling a 2D reservoir to 0D states has already been shown to lead to fast gain recovery in semiconductor optical amplifiers.[11,33]

The coupling strength and thus the enhanced decay are tunable over the spatial separation between the nanostructures. The modeled rate equation system describes experimental data approximating the transfer time constants which correspond to the coupling strength. Additionally, our model showed an excitation dependence of the quenching on the excitation caused by Pauli blocking of occupied states in the SK QDs.

The observed dynamical properties of the combined SK QD and SML system can be exploited in several ways, e.g., by engineering the enhanced depopulation rates of the SML stack or taking advantage of the additional filling channel into the QDs.

ACKNOWLEDGMENTS

This work was supported by the German Research Foundation (DFG) within the Collaborative Research Center (SFB 787). The authors thank Nicolai B. Grosse and Nina Owschimikow for support and fruitful discussions.

*thomas.switaiski@tu-berlin.de
†http://www.ioap.tu-berlin.de/menue/arbeitsgruppen/ag_we; ulrike.woggon@tu-berlin.de

[1] J. Lee, V. C. Sundar, J. R. Heine, M. G. Bawendi, and K. F. Jensen, Adv. Mater. **12**, 1102 (2000).
[2] Y. Arakawa, IEEE J. Sel. Top. Quantum Electron. **8**, 823 (2002).
[3] U. Woggon, W. Petri, A. Dinger, S. Petillon, M. Hetterich, M. Grün, K. P. O'Donnell, H. Kalt, and C. Klingshirn, Phys. Rev. B **55**, 1364 (1997).
[4] V. I. Klimov, A. A. Mikhailovsky, S. Xu, A. Malko, J. A. Hollingsworth, C. A. Leatherdale, H.-J. Eisler, and M. G. Bawendi, Science **290**, 314 (2000).
[5] Y. Cao and U. Banin, J. Am. Chem. Soc. **122**, 9692 (2000).
[6] N. N. Ledentsov, I. L. Krestnikov, M. V. Maximov, S. V. Ivanov, S. L. Sorokin, P. S. Kopev, Z. I. Alferov, D. Bimberg, and C. M. Sotomayor Torres, Appl. Phys. Lett. **69**, 1343 (1996).
[7] P. Borri, W. Langbein, S. Schneider, U. Woggon, R. L. Sellin, D. Ouyang, and D. Bimberg, Phys. Rev. Lett. **87**, 157401 (2001).
[8] N. Kirstaedter, N. Ledentsov, M. Grundmann, D. Bimberg, V. Ustinov, S. Ruvimov, M. Maximov, P. Kop'ev, Z. Alferov, U. Richter, P. Werner, U. Gösele, and J. Heydenreich, Electron. Lett. **30**, 1416 (1994).
[9] D. Bimberg, M. Grundmann, F. Heinrichsdorff, N. Ledentsov, V. Ustinov, A. Zhukov, A. Kovsh, M. Maximov, Y. Shernyakov, B. Volovik, A. Tsatsulnikov, P. Kopev, and Z. Alferov, Thin Solid Films **367**, 235 (2000).
[10] D. J. Mowbray and M. S. Skolnick, J. Phys. D **38**, 2059 (2005).
[11] J. Gomis-Bresco, S. Dommers, V. V. Temnov, U. Woggon, M. Laemmlin, D. Bimberg, E. Malic, M. Richter, E. Schöll, and A. Knorr, Phys. Rev. Lett. **101**, 256803 (2008).
[12] Z. Xu, Y. Zhang, J. M. Hvam, J. Xu, X. Chen, and W. Lu, Appl. Phys. Lett. **89**, 013113 (2006).
[13] Z. Xu, Y. Zhang, A. Tackeuchi, Y. Horikoshi, and J. M. Hvam, Appl. Phys. Lett. **92**, 063103 (2008).
[14] T. Niermann, F. Kießling, M. Lehmann, J.-H. Schulze, T. D. Germann, K. Pötschke, A. Strittmatter, and U. W. Pohl, J. Appl. Phys. **112**, 083505 (2012).
[15] I. L. Krestnikov, N. N. Ledentsov, A. Hoffmann, and D. Bimberg, Phys. Status Solidi A **183**, 207 (2001).
[16] T. Inoue, M. Asada, N. Yasuoka, O. Kojima, T. Kita, and O. Wada, Appl. Phys. Lett. **96**, 211906 (2010).
[17] P. Ridha, L. H. Li, M. Mexis, P. M. Smowton, J. Andrzejewski, G. Sek, J. Misiewicz, E. P. O'Reilly, G. Patriarche, and A. Fiore, IEEE J. Quantum Electron. **46**, 197 (2010).
[18] M. Motyka, G. Sek, K. Ryczko, J. Andrzejewski, J. Misiewicz, L. H. Li, A. Fiore, and G. Patriarche, Appl. Phys. Lett. **90**, 181933 (2007).
[19] T. Kita, N. Tamura, O. Wada, M. Sugawara, Y. Nakata, H. Ebe, and Y. Arakawa, Appl. Phys. Lett. **88**, 211106 (2006).
[20] L. Lester, A. Stintz, H. Li, T. Newell, E. Pease, B. Fuchs, and K. Malloy, IEEE Photonics Technol. Lett. **11**, 931 (1999).
[21] A. Lenz, H. Eisele, J. Becker, J.-H. Schulze, T. D. Germann, F. Luckert, K. Pötschke, E. Lenz, L. Ivanova, A. Strittmatter, D. Bimberg, U. W. Pohl, and M. Dähne, J. Vac. Sci. Technol. B **29**, 04D104 (2011).
[22] L. H. Li, G. Patriarche, M. Rossetti, and A. Fiore, J. Appl. Phys. **102**, 033502 (2007).
[23] A. Lenz, H. Eisele, J. Becker, L. Ivanova, E. Lenz, F. Luckert, K. Pötschke, A. Strittmatter, U. W. Pohl, D. Bimberg, and M. Dähne, Appl. Phys. Express **3**, 105602 (2010).
[24] Z. Xu, D. Birkedal, M. Juhl, and J. M. Hvam, Appl. Phys. Lett. **85**, 3259 (2004).
[25] T. D. Germann, A. Strittmatter, J. Pohl, U. W. Pohl, D. Bimberg, J. Rautiainen, M. Guina, and O. G. Okhotnikov, Appl. Phys. Lett. **92**, 101123 (2008).
[26] F. Hopfer, A. Mutig, M. Kuntz, G. Fiol, D. Bimberg, N. N. Ledentsov, V. A. Shchukin, S. S. Mikhrin, D. L. Livshits, I. L. Krestnikov, A. R. Kovsh, N. D. Zakharov, and P. Werner, Appl. Phys. Lett. **89**, 141106 (2006).
[27] N. N. Ledentsov, D. Bimberg, F. Hopfer, A. Mutig, V. A. Shchukin, A. V. Savel'ev, G. Fiol, E. Stock, H. Eisele, M. Dähne, D. Gerthsen, U. Fischer, D. Litvinov, A. Rosenauer, S. S. Mikhrin, A. R. Kovsh, N. D. Zakharov, and P. Werner, Nanoscale Res. Lett. **2**, 417 (2007).
[28] S. A. Blokhin, N. A. Maleev, A. G. Kuzmenkov, A. V. Sakharov, M. M. Kulagina, Y. M. Shernyakov, I. I. Novikov, M. V. Maximov, V. M. Ustinov, A. R. Kovsh, S. S. Mikhrin, N. N. Ledentsov, G. Lin, and J. Y. Chi, IEEE J. Quantum Electron. **42**, 849 (2006).
[29] N. N. Ledentsov, A. F. Tsatsulnikov, A. Y. Egorov, P. S. Kopev, A. R. Kovsh, M. V. Maximov, V. M. Ustinov, B. V. Volovik, A. E. Zhukov, Z. I. Alferov, I. L. Krestnikov, D. Bimberg, and A. Hoffmann, Appl. Phys. Lett. **74**, 161 (1999).
[30] S. S. Mikhrin, A. E. Zhukov, A. R. Kovsh, N. A. Maleev, V. M. Ustinov, Y. M. Shernyakov, I. P. Soshnikov, D. A. Livshits, I. S.

Tarasov, D. A. Bedarev, B. V. Volovik, M. V. Maximov, A. F. Tsatsul'nikov, N. N. Ledentsov, P. S. Kop'ev, D. Bimberg, and Z. I. Alferov, Semicond. Sci. Technol. **15**, 1061 (2000).

[31]E. A. Jares-Erijman and T. M. Jovin, Nat. Biotechnol. **21**, 1387 (2003).

[32]J. R. Lakowicz, in *Principles of Fluorescence Spectroscopy*, 3rd ed. (Springer, New York, 2006), pp. 443–475.

[33]J. Gomis-Bresco, S. Dommers, V. V. Temnov, U. Woggon, J. Martinez-Pastor, M. Laemmlin, and D. Bimberg, IEEE J. Quantum Electron. **45**, 1121 (2009).